Quantum cluster variational method and phase diagram of the quantum ferromagnetic J_1-J_2 model

E. Domínguez,[*] C. E. Lopetegui,[†] and Roberto Mulet[‡]
Group of Complex Systems and Statistical Physics, Department of Theoretical Physics,
University of Havana, CP 10400 La Habana, Cuba

(Received 22 December 2020; revised 15 June 2021; accepted 15 June 2021; published 9 July 2021)

We exploit the quantum cluster variational method (QCVM) to study the J_1-J_2 model for quantum Ising spins. We first describe the QCVM and discuss how it is related to other mean field approximations. The phase diagram of the model is studied at the level of the Kikuchi approximation in square lattices as a function of the ratio between $g = J_2/J_1$, the temperature and the longitudinal and transverse external fields. Our results show that quantum fluctuations may change the order of the transition and induce a gap between the ferromagnetic and the stripe phases. Moreover, when both longitudinal and transverse fields are present, thermal fluctuations and quantum effects contribute to the appearance of a nematic phase.

DOI: 10.1103/PhysRevB.104.014205

I. INTRODUCTION

In most cases of practical interest the solution of problems involving many interacting quantum particles rests on some kind of approximation [1–3]. It is not surprising then that an important fraction of the theoretical work in condensed matter physics is concerned with the development of such approximations and the test of the predictions derived from them. Many of these techniques are similar in spirit; they improve over the simplest mean field approximation to the problem including correlations, and/or interactions between clusters of variables. Among the most celebrated approximations, although certainly not the only ones, we could mention, the effective field theory (EFT) [4], the cluster mean field (CMF) [5,6], and the correlated cluster mean field [7–9]. The quantum cluster variational method (QCVM) [10], inserts into this family in a novel way: it allows the presence of disorder in the model, establishing a clear distinction between average case scenarios and computations on single instances, and connecting with message passing algorithms developed in computer science and information theory [11].

QCVM has its roots in previous results from Morita and Tanaka [12,13] that starting from a pure variational approximation to the free energy of finite dimensional systems derived a set of closed equations for the order parameters of a quantum problem defined by a Hamiltonian. Within this formulation, the resulting set of equations is usually solved assuming the existence of specific symmetries for the order parameter of the model. QCVM goes a step further, extending an approach previously developed for classical disordered models [14–16] to connect these variational approximations with message passing equations in finite dimensional systems. The solutions of these equations can be computed either self-consistently in specific instances of the problem or on average over the disorder [10,16]. QCVM also generalizes to finite dimensional lattices the work done by [17–24], that used message passing algorithms to solve quantum disordered problems in systems with treelike topologies.

In this work we exploit the QCVM to study the phase diagram of the quantum J_1-J_2 model in the presence of external fields. This model belongs to an extensively studied family of similar systems where competing interactions induce exotic phases at low temperatures. This includes systems with short range ferromagnetic and long range dipolar interactions [25–32], long range Coulomb interactions [33], and two-dimensional dipolar Fermi gases [34–36].

The J_1-J_2 model has captured special attention both because of its apparent simplicity, and because of its resemblance to real materials. The classical version has been studied extensively [37–45] but the quantum version has turned out to be harder to crack. Mainly, because quantum fluctuations add complexity to the inherent frustration of the model inducing a zoology of exotic phases: stripelike phases, columnar antiferromagnetic phases, Néel antiferromagnetic phases, spin-liquid phases, and spin nematic phases have been theoretically predicted [39,46–52]. Some of them, like stripes and Néel antiferromagnets, have been experimentally observed [53–55] while others, like the spin nematic phase and the spin-liquid phase, lack conclusive experimental observations but keep the interest of experimentalists [47,56].

Our intention in this work is twofold. On one hand, to test the quantum cluster variational method in a quantum model with competing interactions. On the other, to unveil the effect of quantum fluctuations on the phase diagram of the ferromagnetic J_1-J_2 model with competitive interactions. We study this model extensively as a function of the ratio $g = J_2/J_1$, the temperature T, and external fields. We show that the approximation captures a rich phenomenology of phases and phase transitions.

The work is organized as follows. In the next section we present the model and summarize some of the known results of the literature. We continue introducing the quantum cluster variational method and how it applies to the J_1-J_2 model. In

---

[*] eduardo@fisica.uh.cu

[†] carlosernestolopetegui@gmail.com

[‡] mulet@fisica.uh.cu

this section we also discuss how QCVM is connected with other mean field methods in the literature. Then, we show and discuss the results of our computations for the J_1-J_2 model. In the last section we present the conclusions of our work.

II. THE MODEL

The quantum J_1-J_2 model is one of the most studied models of magnetic materials displaying frustration and is defined by the Hamiltonian

$$\hat{\mathcal{H}} = -\sum_{\langle ij\rangle} J_1 \hat{\sigma}_i^x \hat{\sigma}_j^x - \sum_{\langle\langle ij\rangle\rangle} J_2 \hat{\sigma}_i^x \hat{\sigma}_j^x - \sum_{(i)} \vec{h}_i \cdot \vec{\sigma}_i, \tag{1}$$

where $\langle ij\rangle$ stand for the nearest neighbors in the square lattice and $\langle\langle ij\rangle\rangle$ for the next-nearest neighbors, and the external field $\vec{h}_i$ may point to an arbitrary direction. Here we focus our attention on the model with nearest-neighbor interaction J_1 greater than zero (ferromagnetic), and $J_2 \leqslant 0$. The latter induces the frustration into the model. Since the preferred direction of the system is labeled x, quantum effects appear when the transverse field h_z is different from zero.

In the absence of a longitudinal field the model presents invariance up to the simultaneous rotation of a sublattice and the change of sign of the first neighbors interaction. So, the phase diagrams that are obtained in this scenario (Secs. IV A and IV B), are equivalent to the ones that may be obtained for the antiferromagnetic realization of the model. Indeed, references are mentioned in the Introduction in which indistinctly one or the other realizations are used, this being not a problem as long as they deal only with thermal fluctuation in zero field scenario or transverse field quantum fluctuations. Nevertheless, as soon as we tune a longitudinal field, this symmetry is broken and disparate results can be observed for both versions.

The classical model ($h_z = 0$) has been largely studied [37–41,43–45]. However, also there are some questions that remain open. For example, while for values of $g = \frac{|J_2|}{J_1}$ slightly greater than 0.5 the transition is discontinuous, Monte Carlo studies [43,44] suggest a continuous transition for $g \sim 1$. In a paper by Jin *et al.* [45], the existence of a pseudo-first-order transition in the range $g_c \leqslant g \lesssim 1$ is reported, with $g_c = 0.67$. They found that the critical exponents vary continuously between those of the four-state Potts model at $g = g_c$ to those of the Ising model for $g \to \infty$.

Recently, researchers paid attention also to the effect of external magnetic fields and demonstrated the presence of a nematic phase [39,40], with slight differences, at low temperatures, between the two studies. This nematic phase is characterized by the presence of orientational order and the lack of positional order and has been reported experimentally [56]. A word of caution here on the use of the term *nematic*. Here we understand it as a phase where the rotational symmetry is broken.

In the present work we report, exploiting QCVM, our own perception of this problem, and show that there is no clear separation between pseudo- and actual first-order behavior. Moreover, we studied the combined effect of transverse and longitudinal fields to understand the role played by quantum or thermal fluctuations in the order of these transitions.

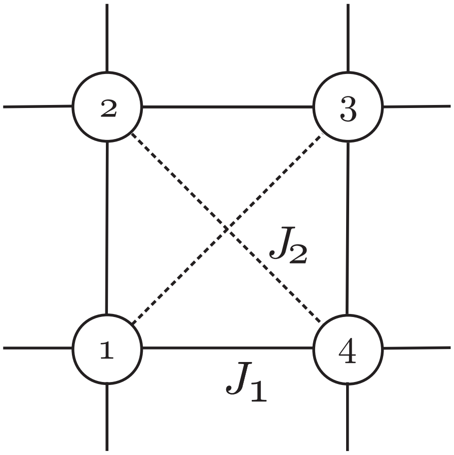

FIG. 1. Convention used in the definition of the order parameters.

We explore the behavior of three order parameters [39,40]. First, we define two positional order parameters which measure the breaking in the translational symmetry of the lattice in two possible directions:

$$M_x = \frac{|m_1^x - m_4^x|}{2}, \tag{2}$$

$$M_y = \frac{|m_1^x - m_2^x|}{2}, \tag{3}$$

where m_i^x refers to the mean magnetization along the preferred direction of the system, of the site i, inside a given plaquette, following the convention shown in Fig. 1.

While translational order parameters are enough to determine the presence of stripes, they are not suited to detect the breaking of the rotational symmetry of the lattice. They take the same values in a paramagnetic and a nematic phase, yet the nematic phase shows a structure of the correlations similar to that of the stripes. This is natural if we think about this phase as an intermediate one in between the completely symmetric paramagnetic phase and the ordered stripes phase. Therefore, to characterize the nematic behavior we introduced an orientational order parameter defined as

$$Q = \frac{|l_{12} + l_{34} - l_{14} - l_{23}|}{4}, \tag{4}$$

where l_{ij} represents the correlation between sites i and j in the plaquette. All the order parameters are in the range $0 \leqslant \{Q, M_x, M_y\} \leqslant 1$.

III. MEAN FIELD APPROXIMATIONS AND QUANTUM CLUSTER VARIATIONAL METHOD

In order to compute the order parameters relevant for the J_1-J_2 model it is fundamental to obtain a good approximation of at least local magnetizations and correlations of neighboring spins. These quantities can be found from a knowledge of the local density matrices describing the joint statistics of these spins.

With a cluster expansion the free energy is approximated as a sum of contributions of selected regions or groups of variables. Each term of the sum depends on the local density matrix of the corresponding variables (spins). These regions are typically chosen to balance the accuracy and the computational cost of the calculations. The resulting approximated expression is to be understood as variational in terms of the local densities. The quality of the final results depends directly on the choice of regions, their size in relation to the correlation length, and how much mean field is put into the treatment of effective interactions and correlation between regions.

Among the many cluster approximations appearing in the literature, the approach known as cluster variational method or CVM is remarkable because of the systematic treatment of different levels of complexity [57,58]. In a natural way one can choose free-energy expansions ranging from naive mean field, a Bethe approximation, or more involved structures. A quantum extension of such ideas, QCVM, was developed in [12,13] and more recently expanded in [10]. In particular, we are interested in a construction called Kikuchi approximation. The Kikuchi free energy F_{Kik} consists of a sum of local free energies of all the square unit cells (p), the interacting pairs (l) formed by the overlap of neighbor cells [59], and all the contributions from single spins (s):

$$F_{\text{Kik}} = \sum_p c_p F_p + \sum_l c_l F_l + \sum_s c_s F_s. \tag{5}$$

The local free-energy terms are defined the usual way

$$F_r = \text{Tr}[\hat{\mathcal{H}}_r \hat{\rho}_r] + T\ \text{Tr}[\hat{\rho}_r \ln \hat{\rho}_r], \tag{6}$$

where r may label a plaquette, link, or spin region. The numbers c_p, c_l, c_s are weight factors that compensate the effect of overlap between regions. Due to overlaps, the contribution of some variables might be under- or over-represented if the weight factors were absent. For the case of interest here, $c_p = 1, c_l = -1, c_s = 1$.

The minimization of the functional F_{Kik} should be done under certain constraints. In addition to the usual normalization conditions, $\text{Tr}[\hat{\rho}_r] = 1$, the consistency between different regions must be enforced explicitly. For all plaquettes $p = \langle ijkm\rangle$ and any of its forming links $l = \langle ij\rangle$ one could demand that the partial trace over spins k and m equals the link density $\hat{\rho}_l$:

$$\text{Tr}_{p\setminus l}[\hat{\rho}_p] = \hat{\rho}_l. \tag{7}$$

Moreover, every link distribution $\hat{\rho}_l$ could be forced to marginalize onto the corresponding spin densities $\hat{\rho}_i$ and $\hat{\rho}_j$:

$$\text{Tr}_j[\hat{\rho}_l] = \hat{\rho}_i; \quad \text{Tr}_i[\hat{\rho}_l] = \hat{\rho}_j. \tag{8}$$

However, numerical results [10] have shown that the above constraint scheme is too restrictive. It turns out that the minimization gives much more accurate results if consistency is enforced only in the direction of the spin-spin interactions. In this model, where interactions exist only in the OX direction, it amounts to relaxing (7) to the set of equations:

$$\left.\begin{aligned} \text{Tr}\big[\hat{\rho}_p\hat{\sigma}_i^x\hat{\sigma}_j^x\big] &= \text{Tr}\big[\hat{\rho}_l\hat{\sigma}_i^x\hat{\sigma}_j^x\big]\\ \text{Tr}\big[\hat{\rho}_p\hat{\sigma}_i^x\big] &= \text{Tr}\big[\hat{\rho}_l\hat{\sigma}_i^x\big]\\ \text{Tr}\big[\hat{\rho}_p\hat{\sigma}_j^x s\big] &= \text{Tr}\big[\hat{\rho}_l\hat{\sigma}_j^x\big] \end{aligned}\right\} \quad \forall\ p, \forall\ l = \langle ij\rangle \in p, \tag{9}$$

$$\left.\begin{aligned} \text{Tr}\big[\hat{\rho}_l\hat{\sigma}_i^x\big] &= \text{Tr}\big[\hat{\rho}_i\hat{\sigma}_i^x\big]\\ \text{Tr}\big[\hat{\rho}_l\hat{\sigma}_j^x\big] &= \text{Tr}\big[\hat{\rho}_j\hat{\sigma}_j^x\big] \end{aligned}\right\} \quad \forall ye\ l = \langle ij\rangle. \tag{10}$$

We are now in position to write a Lagrange function that includes the conditions (9) and (10) by means of suitable Lagrange multipliers $\hat{\lambda}$, $\hat{\gamma}$:

$$\begin{aligned} L[\{\hat{\rho}_p\}, \{\hat{\rho}_l\}, \{\hat{\rho}_s\}] = F_{\text{Kik}} &+ \sum_p \sum_{l\in p} \text{Tr}_l[\hat{\lambda}_{p\to l}(\hat{\rho}_l - \text{Tr}_{p\setminus l}[\hat{\rho}_p])]\\ &+ \sum_l \sum_{s\in l} \text{Tr}_s[\hat{\gamma}_{l\to s}(\hat{\rho}_s - \text{Tr}_{l\setminus s}[\hat{\rho}_l])]\\ &+ \text{normalization conditions.} \end{aligned} \tag{11}$$

To conform to (9) and (10), it suffices to introduce the parametrization [60]:

$$\hat{\lambda}_{p\to l} = C_{p\to l}\hat{\sigma}_i^x\hat{\sigma}_j^x + c_{p\to i}\hat{\sigma}_i^x + c_{p\to j}\hat{\sigma}_j^x, \tag{12}$$

$$\hat{\gamma}_{l\to i} = d_{l\to i}\hat{\sigma}_i^x. \tag{13}$$

It is enough to make C, c, d all real to guarantee that $\hat{\lambda}$ and $\hat{\gamma}$ are Hermitian, and consequently, that L is real. Moreover, this parametrization ensures that the operators $\hat{\rho}$ that satisfy the stationary condition are all positive, which is the fundamental property of density matrices (in addition to a unit trace, of course).

We will say that the value of the Lagrange function $L[\hat{\rho}_r]$ is stationary with respect to a change in the density $\hat{\rho}_r$ if the linear part of the expansion of $L[\hat{\rho}_r + \epsilon\delta\hat{\rho}_r]$, in powers of ϵ, is zero. The operator $\delta\hat{\rho}_r$ is arbitrary but should be Hermitian, traceless, and small enough to keep $\hat{\rho}_r + \epsilon\delta\hat{\rho}_r$ as a valid density operator. The Lagrange function will be stationary with respect to the set of all densities $\{\hat{\rho}_p\}, \{\hat{\rho}_l\}, \{\hat{\rho}_s\}$, by definition, if it is stationary in each one of them. The stationarity condition can be summarized in the following formula:

$$\left.\frac{\partial L[\hat{\rho}_r + \epsilon\delta\hat{\rho}_r]}{\partial\epsilon}\right|_{\epsilon=0} = 0 \quad \forall\ \text{region}\ r. \tag{14}$$

As an example, let us work out the form of the density matrix of an arbitrary spin s_0 at the stationary point. The part of L that depends on a given $\hat{\rho}_{s_0}$ is

$$\begin{aligned} &\text{Tr}\big[\hat{\rho}_{s_0}\hat{\mathcal{H}}_{s_0}\big] + T\ \text{Tr}\big[\hat{\rho}_{s_0}\ln\hat{\rho}_{s_0}\big] + \alpha_{s_0}\big(\text{Tr}\big[\hat{\rho}_{s_0}\big] - 1\big)\\ &\quad + \sum_{l\ni s_0} \text{Tr}\big[\hat{\gamma}_{l\to s_0}\big(\hat{\rho}_{s_0} - \text{Tr}_{l\setminus s_0}[\hat{\rho}_l]\big)\big]. \end{aligned} \tag{15}$$

In (15) the only term that is somewhat involved to expand to first order in ϵ, when evaluating $L[\hat{\rho}_{s_0} + \epsilon\delta\hat{\rho}_{s_0}]$, is the one with the logarithm. The trick is to use perturbation theory to write the eigenvalues $r_i(\epsilon)$ of $\hat{\rho}_{s_0} + \epsilon\delta\hat{\rho}_{s_0}$ using the eigenvalues and eigenvectors $\{r_i, |r_i\rangle\}$ of $\hat{\rho}_{s_0}$:

$$r_i(\epsilon) = r_i + \epsilon\ \big(\delta\hat{\rho}_{s_0}\big)_{ii} + o(\epsilon), \tag{16}$$

$$\big(\delta\hat{\rho}_{s_0}\big)_{ii} = \langle r_i|\delta\hat{\rho}_{s_0}|r_i\rangle. \tag{17}$$

The trace with the logarithm is therefore written as

$$\begin{aligned} \text{Tr}\big[\big(\hat{\rho}_{s_0} + \epsilon\delta\hat{\rho}_{s_0}\big)\ln\big(\hat{\rho}_{s_0} + \epsilon\delta\hat{\rho}_{s_0}\big)\big] &= \sum_i r_i(\epsilon)\ln r_i(\epsilon)\\ &= \sum_i r_i\ln r_i + \epsilon\sum_i \big(\delta\hat{\rho}_{s_0}\big)_{ii}(\ln r_i + 1) + o(\epsilon)\\ &= \text{Tr}\big[\hat{\rho}_{s_0}\ln\hat{\rho}_{s_0}\big] + \epsilon\ \text{Tr}\big[\delta\hat{\rho}_{s_0}\ln\hat{\rho}_{s_0}\big] + o(\epsilon). \end{aligned} \tag{18}$$

In (18) we used that $\delta\hat{\rho}_{s_0}$ has a null trace. From the results above it is not hard to deduce the linear expansion of $L[\hat{\rho}_{s_0}+\epsilon\delta\hat{\rho}_{s_0}]$:

$$L\big[\hat{\rho}_{s_0}+\epsilon\delta\hat{\rho}_{s_0}\big]=L\big[\hat{\rho}_{s_0}\big]+\epsilon\mathrm{Tr}\big[\delta\hat{\rho}_{s_0}\hat{\mathcal{H}}_{s_0}\big] + \epsilon\mathrm{Tr}\left[\delta\hat{\rho}_{s_0}\left(T\ln\hat{\rho}_{s_0}+\sum_{l\ni s_0}\hat{\gamma}_{l\to s_0}\right)\right]+o(\epsilon). \tag{19}$$

The stationarity condition applied to (19) implies the following relation:

$$\mathrm{Tr}\left[\delta\hat{\rho}_{s_0}\left(\hat{\mathcal{H}}_{s_0}+T\ln\hat{\rho}_{s_0}+\sum_{l\ni s_0}\hat{\gamma}_{l\to s_0}\right)\right]=0. \tag{20}$$

Now we use that $\delta\hat{\rho}_{s_0}$ is an arbitrary traceless Hermitian operator to state that the part in parentheses in (20) is at most a constant times the identity, and therefore, $\hat{\rho}_{s_0}$ must have the form

$$\hat{\rho}_{s_0}=\frac{1}{\mathcal{Z}_{s_0}}\exp\left(-\beta\left[\hat{\mathcal{H}}_{s_0}+\sum_{l\ni s_0}\hat{\gamma}_{l\to s_0}\right]\right) \tag{21}$$

with $\beta=1/T$. The condition $\mathrm{Tr}[\hat{\rho}_{s_0}]=1$ determines the value of $\mathcal{Z}_{s_0}$. The form of (21) resembles a Boltzmann distribution where an effective interaction given by the Lagrange multipliers $\hat{\gamma}_{l\to s_0}$ is added to the original local Hamiltonian.

The same procedure that leads to (21) can be used to find expressions for the rest of the density operators, that is, for pair and plaquette densities. The general structure will be the same: a Boltzmann distribution where the local Hamiltonian is modified by a number of effective interactions. These appear due to the consistency relations between regions and via the corresponding Lagrange multipliers. We skip these derivations and only write the final expressions for the Kikuchi approximation:

$$\hat{\rho}_s=\frac{1}{\mathcal{Z}_s}\exp\left(-\beta\left[\hat{\mathcal{H}}_s+\sum_{l\ni s}\hat{u}_{l\to s}\right]\right),$$

$$\hat{\rho}_l=\frac{1}{\mathcal{Z}_l}\exp\left(-\beta\left[\hat{\mathcal{H}}_l+\sum_{p\ni l}\hat{U}_{p\to l}+\sum_{\substack{l'\ni i\\ l'\neq l}}\hat{u}_{l'\to i}+\sum_{\substack{l'\ni j\\ l'\neq l}}\hat{u}_{l'\to j}\right]\right),$$

$$\hat{\rho}_p=\frac{1}{\mathcal{Z}_p}\exp\left(-\beta\left[\hat{\mathcal{H}}_p+\sum_{l\in p}\sum_{\substack{p'\ni l\\ p'\neq p}}\hat{U}_{p'\to l}+\sum_{i\in p}\sum_{\substack{l'\ni i\\ l'\notin p}}\hat{u}_{l'\to i}\right]\right). \tag{22}$$

In (22) we used a linear transformation to write $\hat{\lambda}_{p\to l}$ and $\hat{\gamma}_{l\to i}$ as a function of new parameters $\hat{U}_{p\to l}$ and $\hat{u}_{p\to i}$, respectively. These changed variables will of course inherit the structure of the originals [see (12) and (13)]:

$$\hat{U}_{p\to l}=-U_{p\to l}\hat{\sigma}_i^x\hat{\sigma}_j^x-u_{p\to i}\hat{\sigma}_i^x-u_{p\to j}\hat{\sigma}_j^x,$$
$$\hat{u}_{l\to s}=-u_{l\to s}\hat{\sigma}_s^x. \tag{23}$$

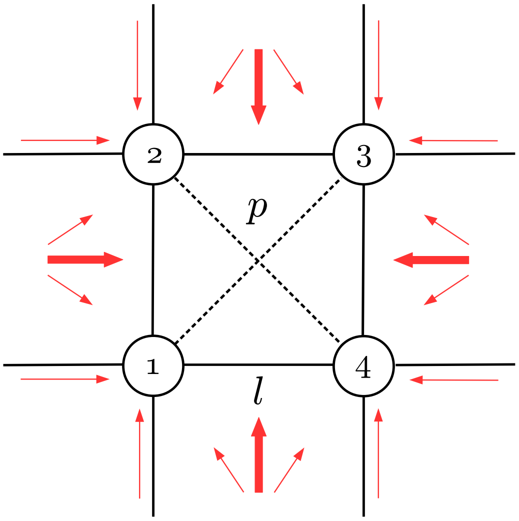

FIG. 2. Effective fields involved in the computation of $\hat{\rho}_p$ for a plaquette p, according to formula (22). Diagonal interactions for plaquettes other than p are not shown for simplicity.

The form of (12), (13), and (23) suggests that the Lagrange multiplier can be interpreted as effective local fields and a contribution to the interaction constants between spins when their explicit form is put into Eqs. (22). The plaquette-to-pair $\hat{U}_{p\to l}$ is composed of a term that adds to the $J_1\hat{\sigma}_i^x\hat{\sigma}_j^x$ part of the original local Hamiltonian, and two effective fields $u_{p\to i}, u_{p\to j}$ acting on the spins of the pair $l=\langle ij\rangle$. On the other hand, the pair-to-spin $\hat{u}_{l\to s}$ is formed by an effective field on $\hat{\sigma}_s^x$, for every spin s that belongs to l. The role of these extra fields is to guarantee the consistency between the distributions, according to the restrictions imposed to the variational function.

The nature of the constraints directly implies that no effective fields (or modification to interaction constants) act in the transverse (OZ) direction. The reason being that no consistency is demanded on this axis. As a consequence, moments and correlations in the OZ direction may differ if computed from different local densities. Since all the observables we study here are in OX, where consistency holds, this discrepancy is not a serious complication.

A graphical representation of the effective fields entering the formula (22) for the plaquette density operator $\hat{\rho}_p$ is shown in Fig. 2. Effective fields are drawn as arrows, placed according to the regions they are related to. For example, the arrows standing parallel to the edges of the lattice [nearest neighbors (NN) interactions] correspond to $\hat{u}_{l'\to i}$ terms. The arrows (triplet) pointing from the center of a square to a border pair picture the $\hat{U}_{p'\to l}$ operators. In the same way, Figs. 3 and 4 provide the representation for distributions $\hat{\rho}_l$ and $\hat{\rho}_s$.

The final step to determine the local distributions is to find the value of the effective parameters. Their value is determined by the solution of the set of equations imposed by the consistency relations (9) and (10). The numerical algorithm used to solve these coupled equations is a fixed point iteration, very similar to the classical generalization of the well known belief propagation and is described in detail in [10].

The parameters $\hat{U}_{p'\to l}$ and $\hat{u}_{l'\to i}$, regarded throughout this paper as effective interactions, are in direct correspondence

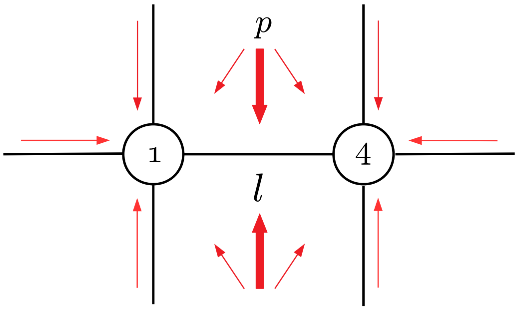

FIG. 3. Effective fields involved in the computation of $\hat{\rho}_l$ for a pair l, according to formula (22). Diagonal interactions are omitted for simplicity.

to the so-called *messages* in the standard belief propagation literature [57]. The *messages* incoming a region are considered to "inform" about the interaction of this region with the surrounding ones and enforce the consistency between them. The term *message passing* is commonly used for the process of fixed point iterations, where one can think of information being exchanged between regions until agreement (convergence) is achieved.

The basic scheme of the algorithm is the following. All effective fields are initialized in an arbitrary way (randomly, uniform, following a certain pattern, etc.). Then, a series of update steps are performed until convergence is achieved [61]. We understand convergence as the situation where the values of the effective fields are such that all the consistency relations are satisfied simultaneously.

Let us describe a typical iteration for the field $\hat{U}_{p\to(14)}$ (upper triplet in Fig. 3). First, compute $\hat{\rho}_p$ using the current value of the fields depicted in Fig. 2. Then, from $\hat{\rho}_p$ determine the correlation $c_{14} = \langle\hat{\sigma}_1^x\hat{\sigma}_4^x\rangle$ and the magnetizations $m_1 = \langle\hat{\sigma}_1^x\rangle$, $m_4 = \langle\hat{\sigma}_4^x\rangle$. The crucial part is to use the consistency condition between $\hat{\rho}_p$ and $\hat{\rho}_{14}$. We should find a value for the three components of $\hat{U}_{p\to(14)}$ (this parameter enters the formula for $\hat{\rho}_{14}$ and *not* $\hat{\rho}_p$) such that the observables computed from the pair distribution $\hat{\rho}_{14}$ match the plaquette predictions:

$$\left\langle\hat{\sigma}_1^x\hat{\sigma}_4^x\right\rangle_{\hat{\rho}_{14}} = c_{14}, \tag{24}$$

$$\left\langle\hat{\sigma}_1^x\right\rangle_{\hat{\rho}_{14}} = m_1, \tag{25}$$

$$\left\langle\hat{\sigma}_1^x\right\rangle_{\hat{\rho}_{14}} = m_4. \tag{26}$$

The three equations above suffice to find the three parameters $\hat{U}_{p\to(14)} \sim (U_{p\to(14)}, u_{p\to 1}, u_{p\to 4})$. The newly found value of $\hat{U}_{p\to(14)}$ is then updated in the lattice [62].

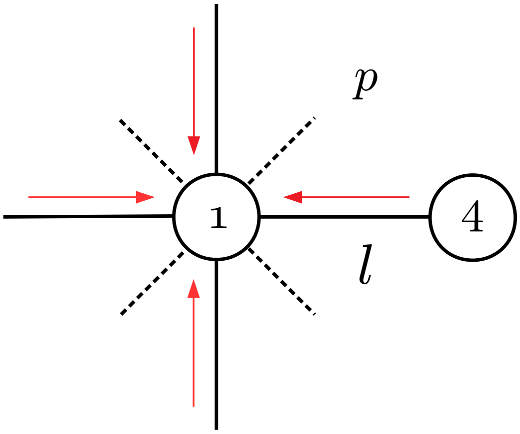

FIG. 4. Effective fields involved in the computation of $\hat{\rho}_s$ for a single spin s ($s = 1$ in this case), according to formula (22). Diagonal interactions are represented only for reference, but no effective field appears on these edges.

Updating a pair-to-spin field, for example $\hat{u}_{(14)\to 1}$, follows a similar recipe. First compute $\hat{\rho}_{l=(14)}$ using the fields of Fig. 3. Then compute the spin 1 magnetization $\langle\hat{\sigma}_1^x\rangle$ using $\hat{\rho}_l$. Finally, find a value $u_{(14)\to 1}$ such that the same magnetization computed with $\hat{\rho}_1$ matches the value computed with the pair distribution.

The algorithm described here assumes that we are using a given realization of the model, that is, that we are computing all the effective fields for every region defined in a $N = L^2$ square lattice. The procedure is general and can handle situations where the external fields applied may not be homogeneous or the interactions change across the lattice. However, since the model in question is translationally invariant, it is reasonable to expect a simplification of the calculations; one would hope this structure is reflected in a translational symmetry of the effective fields. This is indeed the case. If the same values repeat all over the lattice, it is not necessary to solve $O(N)$ equations but only a reduced set. The fields outside a certain region of the lattice can be taken as the same computed inside that region. In this case the numerical procedure looks like a self-consistent iteration. The idea, though, is not that every site in the lattice is equivalent to the rest; that is a too restrictive assumption that would allow only homogeneous states. The correct procedure is to consider the smallest possible structures that, by repetition, can create the patterns observed experimentally. In practice, to generate a pattern of stripes, or an antiferromagnetic checkerboard design, it is enough to consider a square plaquette as the elementary region. For the model studied here we followed both approaches; a specific realization of the lattice solving N equations and the more practical reduced version obtained equivalent results. For generality we will present only simulation results for the first method. On one hand it makes clearer the strength of QCVM for more general situations, and on the other, makes it more transparent when the algorithm does not converge.

To close this section we would like to make a few comments about our choice of the QCVM as the inference method used to compute the local observables of the J_1-J_2 model. Mean field cluster approximations frequently found in the literature [4,63,64] are often based on some kind of variational argument on single site spin magnetizations. In many cases the effect is equivalent to factoring out the correlations as products of single site moments. A more consistent treatment is expected to take into account more structure in the relevant correlations among the system variables. That is precisely the formal advantage of QCVM: by means of the effective interactions the correlations have extra parameters that can be used for tuning. This can lead to more precision in the

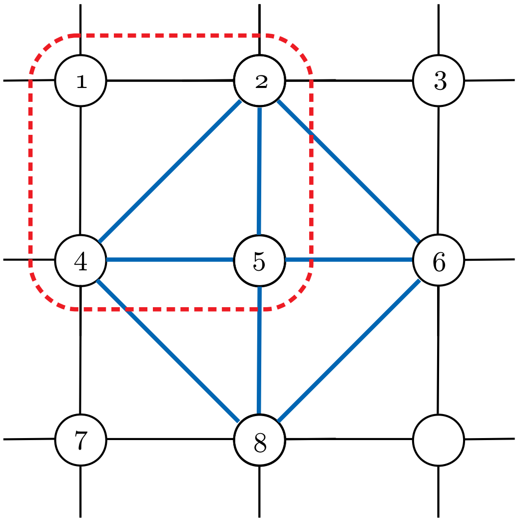

FIG. 5. In red, the standard plaquette region used in the Kikuchi approximation. The rhombic region (2-4-5-6-8) (in blue) represents an alternative choice of plaquette geometry that would generate diagonal pairwise regions and effective fields. Some interactions were not represented in the figure for clarity.

prediction of system properties. A quick test, for example, shows that the CMF of [63] applied to a classical Ising model on a square lattice returns predictions for the para-ferro transition temperature, $T_{\mathrm{CMF}} \approx 3.5$, which is closer to the naive mean field (MF) prediction $T_{\mathrm{MF}} = 4.0$ than to the real value $T_c \approx 2.26$ [65]. Bethe-Peierls approximation or Kikuchi give much more accurate estimates (2.89 and 2.423, respectively; see [58,66,67]). At the plaquette level, the main difference between QCVM and the CMF approximations already mentioned is the inclusion of effective correlation "fields" that modify the spin-spin interaction constant. Also, CMF does not treat all parts of the system on the same footing: intercluster interactions are treated in a different manner than the intracluster ones. The QCVM does not introduce an arbitrary inhomogeneity in the formalism; it handles all interactions and regions equally. Although our purpose is not a thorough comparison, more numerical results for both approximations are mentioned in the Results and Discussion section.

Mean field treatments usually replace real interactions by the interaction with the mean value of certain variables. For example, terms like $J_1\hat{\sigma}_1^x\hat{\sigma}_2^x$ might be roughly approximated by $J_1\hat{\sigma}_1^x\langle\hat{\sigma}_2^x\rangle$ or something similar, which looks like an effective field acting on $\hat{\sigma}_1^x$. QCVM effective fields can be understood in a similar way. With this in mind, we would like to point to what might be a caveat in the choice of regions used in the Kikuchi approximation. Since the overlap of elementary plaquettes corresponds only to NN pairs, the effective fields will only appear for those interactions. Notice, for example, the scheme for the single site distribution $\hat{\rho}_s$ in Fig. 4, where no diagonal effective fields are present. It would be desirable to have a setup where consistency is also forced for diagonal distributions which would then appear as diagonal effective fields. In Fig. 5 the square plaquette used in the current approximation is shown in red. Such plaquettes are formed by spins in a geometry similar to the (1-2-4-5) set. The inclusion of diagonal regions could be achieved if the basic plaquettes are selected with a rhombic shape, including spins in sets like (2-4-5-6-8). This idea is not pursued further in this contribution but we mention it as a possible path to more accurate results.

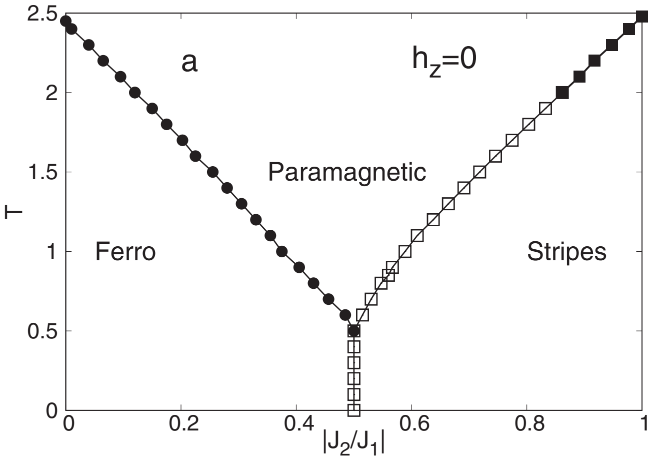

FIG. 6. T vs g phase diagram in the zero field scenario for the J_1-J_2 frustrated ferromagnetic Ising model. Open squares represent discontinuous transitions and filled squares continuous transitions.

IV. RESULTS AND DISCUSSION

A. Summary of the classical model

We start this section presenting the phase diagram of the classical version of the model derived using the cluster variational method [40]. On one hand, it may help to understand better the effects of quantum fluctuations, and on the other it serves as a checking point to probe that the approximation reproduces the known phenomenology of the model.

In short, as shown in Fig. 6, depending on the temperature and the ratio $|J_2|/J_1$ the model may be in one of three phases: ferromagnetic, stripes, or paramagnetic [45]. The lines are guides to the eyes, and the symbols represent the predicted order of the transition: continuous (closed), discontinuous (open).

The ground state in the low $|J_2|$ regime is ferromagnetic, and the system behaves essentially as an Ising ferromagnet with a continuous phase transition between the ferromagnetic and the paramagnetic phases. When $J_2 = 0$ the critical temperature predicted by the approximation is around $T_c^* = 2.425$, which is close to the exact critical value $T_c = 2.26$ [65], and represents an improvement with respect to predictions done in the context of other mean field approximations [63].

On the other branch of the diagram $g = \frac{|J_2|}{J_1} \geqslant 0.5$ the system shows a high temperature paramagnetic phase and a low temperature phase of stripes. However, the line dividing the two phases is characterized by different kinds of phase transitions. Notice that Jin *et al.*, [45] predicted that below $g_c = 0.67$ the transition is discontinuous and above continuous. QCVM provides a similar picture, but with a larger $g_c = 0.86$. Nevertheless we need to remark that the definition of this critical point from numerical simulations is highly nontrivial. For example, in Fig. 7, we show the behavior of the free energy when the parameter g changes. At $T = 1.2$

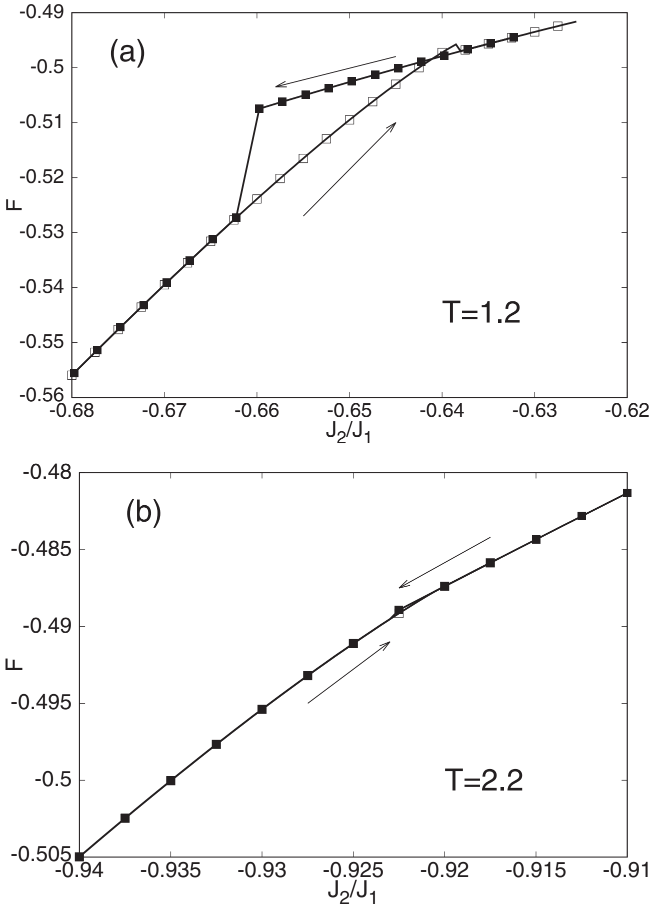

FIG. 7. Free-energy curve for two different temperatures, close to the phase transition. In panel (a), $T = 1.2$, a hysteresis loop, is observed. In panel (b), a well behaved line is observed for $T = 2.2$, close to the transition, which occurs around $g = -0.920$.

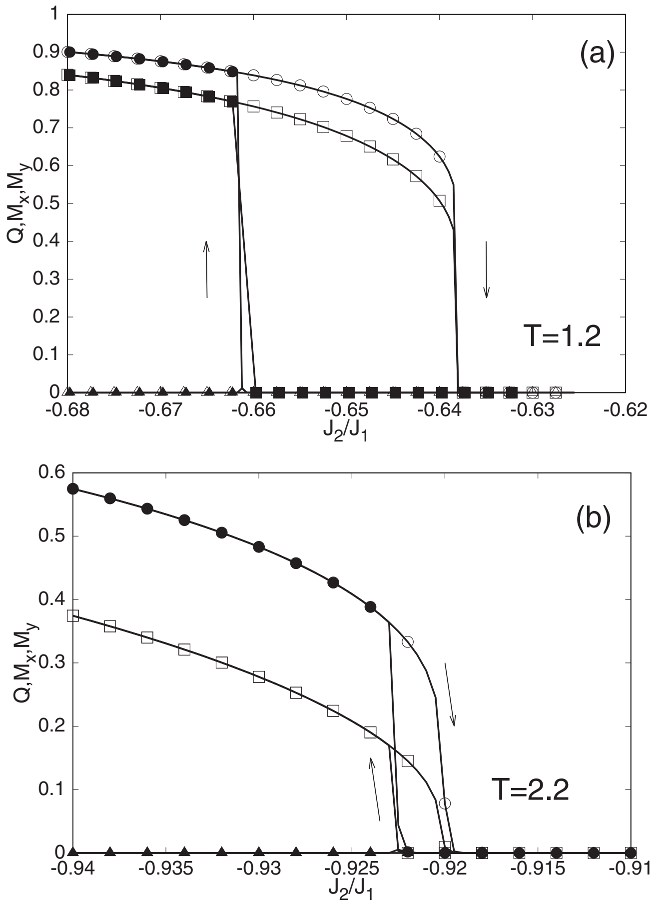

FIG. 8. Behavior of the order parameters at $T = 1.2$ [panel (a)], and $T = 2.2$ [panel (b)], close to the phase transition ($g^* = 0.641$ and $g^* = 0.920$, respectively). Squares represent the orientational order parameter. Circles and triangles stand for the positional order parameters. There are two of them because stripes can form either along the y axis or the x axis.

[Fig. 7(a)], we find a very clear hysteresis loop, a signature of a first order transition. On the other hand, for $T = 2.2$ [Fig. 7(b)], the free-energy dependence is flat, and there is no evidence of any hysteresis. In the rest of the work the order of the phase transitions was determined both by considering the occurrence of hysteresis loops in the free energy and by making an interpolation of the free energy and studying the continuity of its derivative close to the transition as discussed in the previous sections. Results from both methods are equivalent.

This phase diagram is in qualitative agreement with previously reported ones that consider either the ferromagnetic or antiferromagnetic versions of the model [5,43,45,63]. It also represents a quantitative improvement of the predictions if compared with CMF approaches [63]. In particular, it can be observed that the critical temperature in the $J_2 = 0$ ($T_{\mathrm{CVM}} = 2.425$) is closer to the Monte Carlo result ($T_c = 2.26$) than the CMF result: $T_{\mathrm{CMF}} > 3$. Also, for $g = 1$, the reported value of the critical temperature ($T^*_{\mathrm{CVM}} \approx 2.5$), compares better to the Monte Carlo value $T^*_{MC} = 2.082$ reported in [43] than the result obtained by the CMF scheme ($T^*_{\mathrm{CMF}} \approx 4$). On the other hand, the definition of the order of the phase transition is a more subtle issue, and there is an open debate in the literature. Our observations reinforce the widely accepted idea that the transition line for $g < 0.5$, is a continuous one [5,43,45,63], though some debate still remain on this due to MF and EFT predictions [5,68]. The consensus about the $g > 0.5$ branch, i.e., the stripes-paramagnetic transition, is less evident. Jin *et al.* in [45], located it around $g_c = 0.67$, by proving the development of Ashkin-Teller criticality for $g > g_c$. The same authors report a pseudo-first-order behavior for $g_c < g \lesssim 0.9$. This behavior is characterized by the presence of first-order features such as double piked energy histograms in finite size systems, that tend to disappear in the thermodynamic limit [5,45,69]. On the other hand, within the CMF technique [63] reported a critical point at $g^c_{\mathrm{CMF}} \approx 0.66$ improving previous determinations by effective field theory approaches ($g^c_{\mathrm{EFT}} \approx 0.97$). QCVM predicts a larger value, $g^c_{\mathrm{CVM}} \approx 0.87$, and is probably not suitable to distinguish between actual first-order and pseudo-first-order phase transitions by considering only the behavior of the observables.

In Fig. 8 we show the behavior of the orientational and positional order parameters around the transition. For $T = 1.2$, Fig. 8(a), it can be observed a wide hysteresis loop when J_2 increases or decreases and a sharp jump in the order

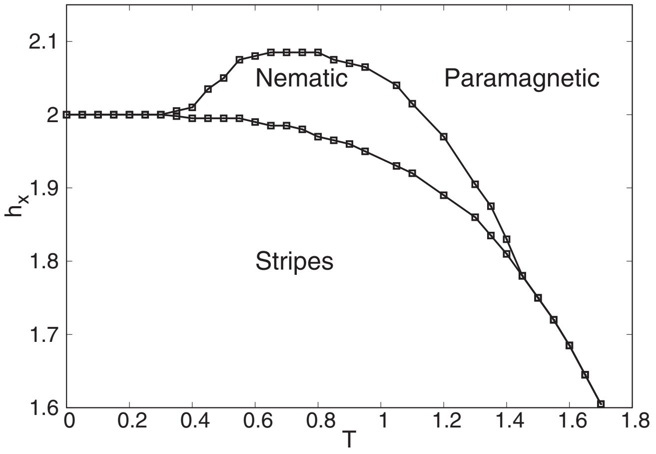

FIG. 9. h_x vs T phase diagram for the classical J_1-J_2 frustrated ferromagnetic Ising model with $J_1 = 1$ and $J_2 = -1$. A nematic phase is present in a narrow region of the phase diagram for large field, and relatively low values of temperature.

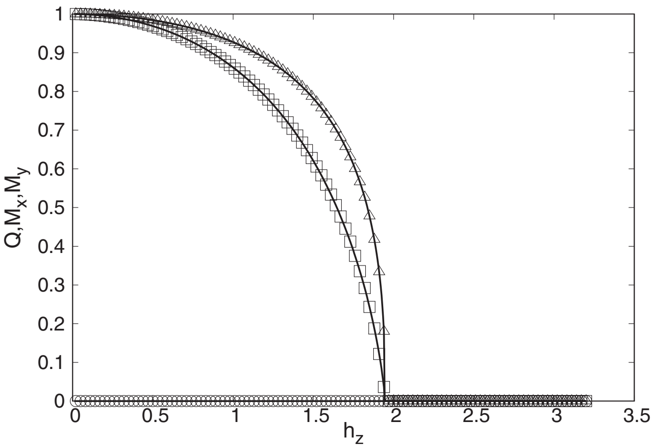

FIG. 10. Behavior of the orientational and positional order parameters for $T = 0.1$, $h_x = 0$, $J_2 = -0.72$, close to a quantum phase transition induced by a transverse field. The critical value of h_z is $h_z^* = 1.945$.

parameter, both indications of a discontinuous transition. On the other hand [Fig. 8(b)], for $T = 2.2$ there is a continuous change in the order parameter when J_2 increases, suggesting a continuous transition. However, there is also a small hysteresis loop suggesting a possible discontinuous transition. We checked that it is rather a consequence of the stability of the paramagnetic solution for this approximation, which is always a valid solution of the fixed point equations.

The richness of this model becomes more evident in the presence of a longitudinal field. In this case [see Fig. 9] for proper values of the temperature and the field a nematic phase separates the paramagnetic phase and the phase of stripes [39,40].

Summarizing, in the absence of external fields the classical J_1-J_2 model presents (depending on the value of J_2) two low temperature phases: ferromagnetic and stripes. Increasing T the ferromagnet behaves essentially like an Ising ferromagnet with a continuous transition to a paramagnetic phase. The phase of stripes may have, depending on J_2, a continuous or discontinuous transition to the paramagnetic phase. On the other hand, and depending on the temperature, in the presence of a longitudinal field the stripes and paramagnetic phases may be separated by a novel nematic region.

B. The role of quantum fluctuations

With the previous understanding of the classical model we now concentrate our attention on the main motivation of our work: the role of quantum fluctuations.

We first explore the behavior of the QCVM at low values of the temperature, $T = 0.1$, and in the absence of the longitudinal field, $h_x = 0$. In this regime, and in the absence of quantum fluctuations, the system is either in a ferromagnetic or in a stripe phase (see Fig. 6). Once the transverse external field is turned on and increased, the system eventually turns paramagnetic with both the orientational and positional order falling to zero as is shown in Fig. 10.

An extensive study of the parameters of the model at low temperatures allows the construction of the h_z-g phase diagram (see Fig. 11). Also in this case the ground state for $g \leqslant 0.5$ is a ferromagnet, and the phase transition is continuous. Moreover, the predicted critical field at $J_2 = 0$, corresponding to the quantum ferromagnetic Ising model, is around $h_z^* = 3.175$ [10], which is close to the exact value $h_{z(c)} = 3.04$ [70]. In the right branch of the diagram, the critical point, where the discontinuous transition between the phase of stripes and the paramagnetic phase becomes continuous, is around $g_c^* \approx 0.64$, with $h_z^* = 1.590$. This value is also similar to the one reported by means of a cluster mean field approach in [63] ($g_c = 0.56$). On the other hand, QCVM for $J_2 = -1$ predicts a critical transverse field $h_z^* = 3.025$, much lower than the one reported in [63], $h_z = 3.658$. In short, we find a wide range of parameters for which a continuous transition is observed, in good agreement with the previous studies [4,63]. Moreover, also the phenomenology of the stripes-paramagnetic transition

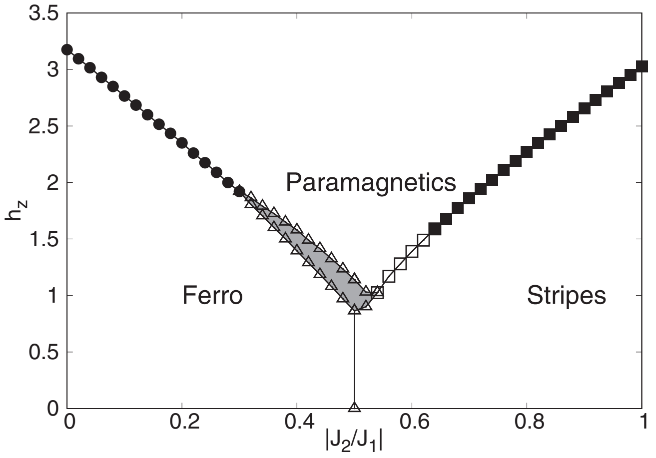

FIG. 11. h_z vs g phase diagram for $T = 0.1$ for the J_1-J_2 frustrated ferromagnetic Ising model. In the stripes-paramagnetic transition a change in the nature of the phase transition occurs around $g_c^* = 0.64$, $h_z = 1.59$. The election of the symbols follows the same convention as in Fig. 6. Triangles represent points in the edge of a nonconvergence region.

provided by the QCVM ($g > 0.5$) shows good qualitative and quantitative agreement with the phenomenology discussed in [63].

The effect of quantum fluctuations reshapes the classical phase diagram T-g presented in Fig. 6. This is shown in Fig. 12. At low values of h_z, quantum fluctuations just extend the range of values of the ratio $|J_2|/J_1$ at which the paramagnetic to stripes transition is continuous i.e., in practice shifting g_c to the left. On the other hand, when the transverse field is large enough ($h_z \geqslant 1$), quantum fluctuations induce a gap between the ferromagnetic and the phase of stripes that is occupied by the paramagnetic phase. In this case, only when the frustration is very small, $J_2 \ll J_1$, or when it is very large, $J_2 \sim J_1$, does the system exhibit actual order at low temperatures.

In both Figs. 11 and 12 we can observe a gray zone separating the ferromagnetic and the paramagnetic phases for the left branch $g \leqslant 0.5$. This is a zone of nonconvergence of the algorithm associated with oscillations due to the existence of two symmetric solutions of the ferromagnetic phase. This zone is discussed in more detail in Appendix.

To summarize, we show in Fig. 13 the T vs h_z phase diagrams for different values of the ratio J_2/J_1. The fact that the thermal and quantum fluctuations driven critical points have different roles makes it possible to characterize three different scenarios. For example, if $J_2/J_1 = -0.58$, we find a full line of discontinuous phase transitions. In the other extreme, when $J_2/J_1 = -1$, there is only a continuous transition, while at intermediate values of the frustration (e.g., $J_2/J_1 = -0.80$), we can observe a line of mixed continuous and discontinuous phase transitions. In other words, in the presence of quantum fluctuations, the frustration favors the occurrence of continuous transitions. As also pointed out in [63], our results support the idea that the intermediate scenario ($g^*_{h_z} < g < g^*_T$) opens the gate for expecting experimental realizations of the model to offer a natural benchmark for achieving quantum annealed criticality [71], i.e., systems that exhibit first-order phase transition at finite temperature but that display continuous quantum phase transition in the quantum regime.

C. Quantum fluctuations in the presence of a longitudinal field

In this section we study the model in the presence of a longitudinal field, h_x. As we already discussed, in the absence of the transverse field, the presence of a longitudinal field induces a nematic phase that separates the paramagnetic and the phase of stripes in a wide range of temperatures (see Fig. 9). We will show that quantum fluctuations make this scenario more plausible with a nematic phase that may penetrate the phase of stripes.

To have a glance at the effect of the longitudinal field in the picture discussed so far, in Fig. 14 we show the behavior of the orientational and positional order parameters against the transverse field for different values of the ratio $g = J_2/J_1$ and the field h_x. It can be observed that depending on the values of g and h_x the system may well have only orientational order but lack translation order ($Q > 0, M = 0$) if h_z is small enough [panel (a)], or alternatively [panel (b)], a phase of stripes for low values of h_z in which both Q and M_x are different

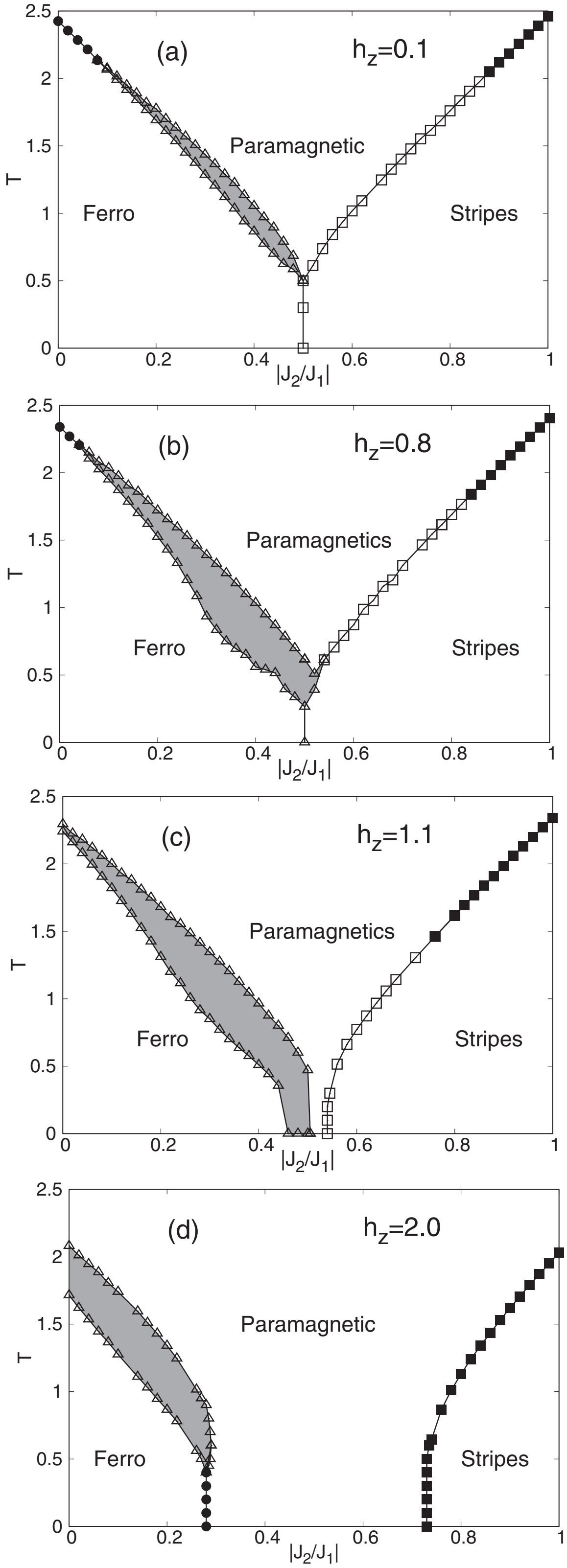

FIG. 12. g vs T phase diagrams in the presence of transverse field. Only for large values of h_z do differences in the phase diagram become relevant. A gap paramagnetic region appears between ordered phases at zero temperature for larger transverse fields. Triangles represent points in the edge of a nonconvergence region.

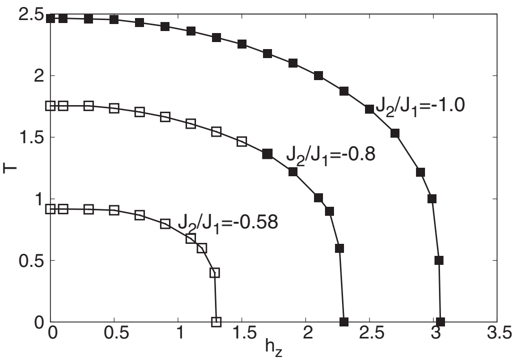

FIG. 13. T vs h_z phase diagrams for different values of J_2. For $J_2 = -0.58$, a line of first-order transition separates the stripes phase from the paramagnetic one. For $J_2 = -1$, a line of second-order transition is observed. For $J_2 = -0.8$, a line with both first- and second-order transition is observed, with a critical point located around $h_z = 1.7$. First-order transition is represented with open squares, and the continuous transition with filled squares.

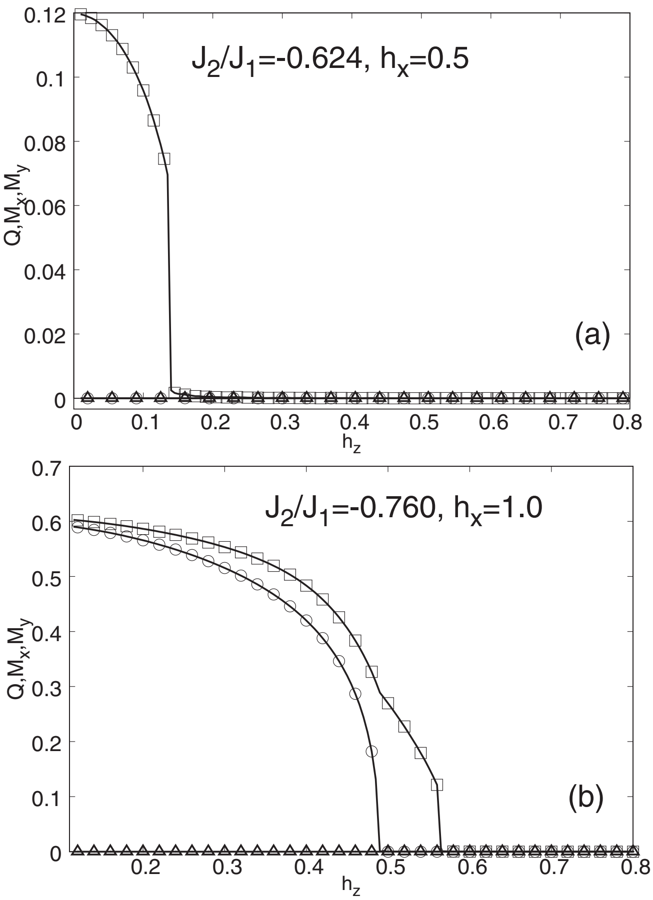

FIG. 14. Behavior of the orientational and positional order paramaters against the transverse field, at the same temperature for two different values of frustration and longitudinal fields. Panel (a) corresponds to the parameters $J_2/J_1 = -0.624$ and $h_x = 0.5$. Panel (b) corresponds to $J_2/J_1 = -0.76$, $h_x = 1.0$.

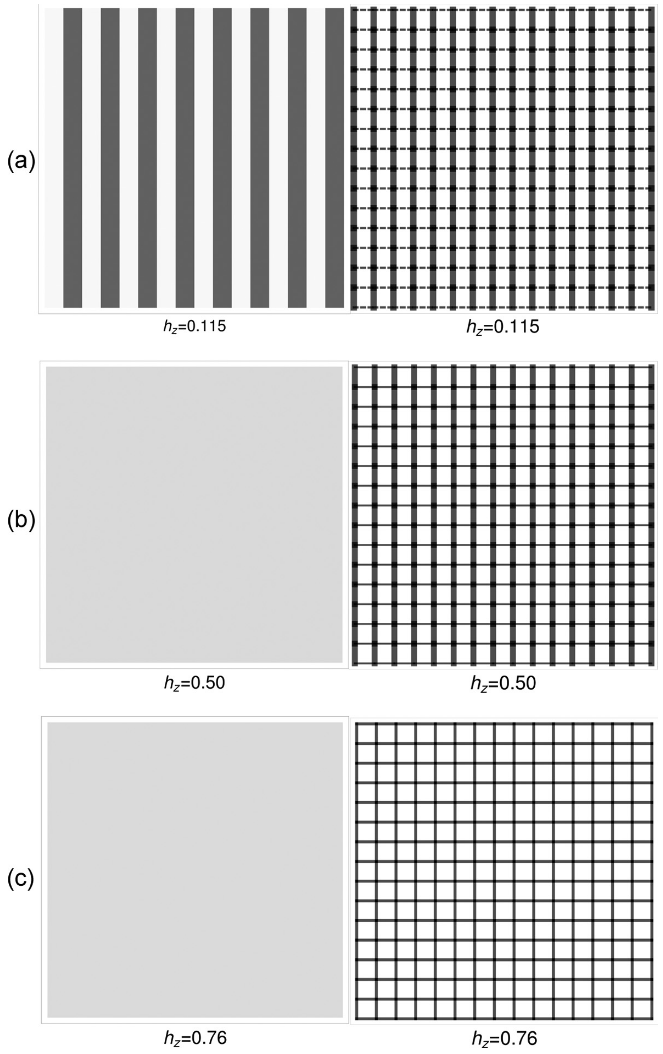

FIG. 15. Magnetization (left) and correlation (right) structure for different values of h_z, with $J_2/J_1 = -0.76$, $h_x = 1.0$, and $T = 0.1$ in a 16×16 lattice. The width of the lines representing the links is proportional to the module of correlation between the sites it joins. On the other hand, negative correlations are represented with dashed lines and positive correlations with continuous lines. The magnetization structure is represented in gray scale so that white corresponds to 1 and black to -1.

from zero. The first is a signature of the nematic phase and a transition from a nematic to a paramagnetic phase due to quantum fluctuations. In the second case, a scenario like that in panel (b) may take place in which, increasing h_z, first the magnetization structure homogenizes, continuously driving the system into a nematic phase, and only later when $h_z \geqslant 0.56$, the orientational order parameter (Q) drops abruptly to zero.

A clearer picture of the situation appears studying the evolution of the correlation and magnetization structure in the lattice as in Fig. 15 for different values of h_z. In this picture the correlation structure is represented using solid (dashed) lines to represent positive (negative) correlations, with a width proportional to their modulus. In Fig. 15(a), we can observe a clear structure of stripes, but with the subtle feature that the global magnetization is not zero, as the sites with positive magnetizations (white stripes) have a larger module than those pointing in the opposite direction. This is a consequence of the application of a field in a direction that breaks the symmetry

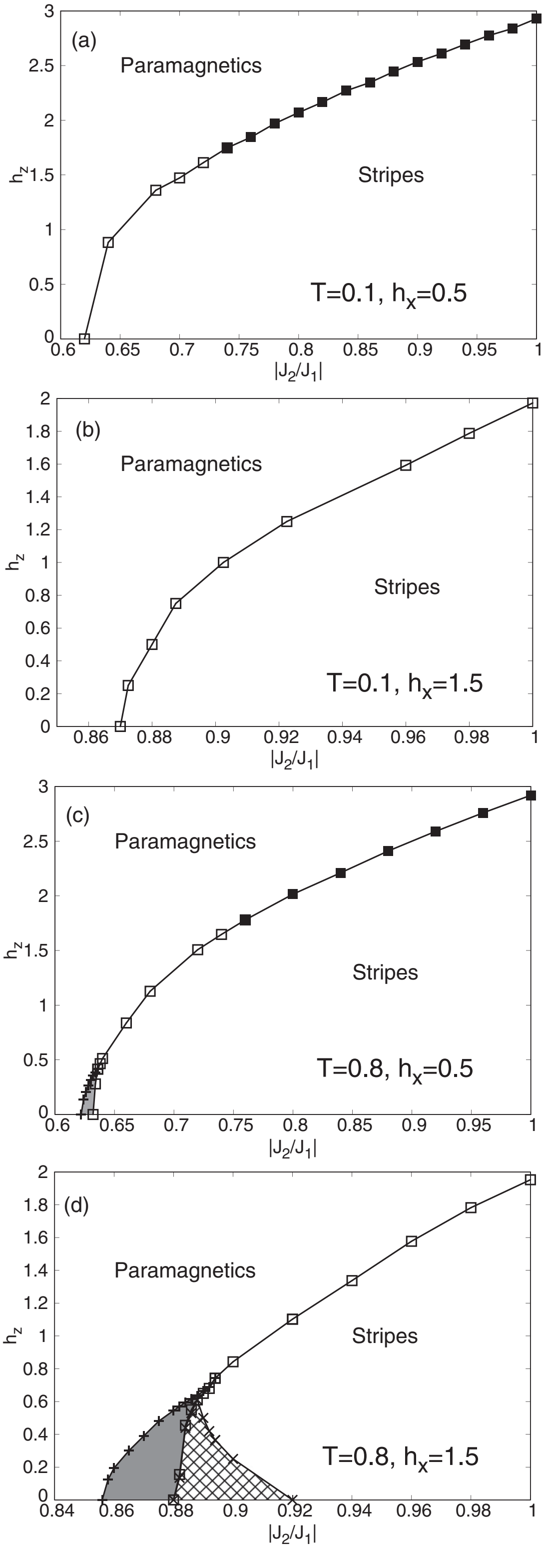

FIG. 16. Phase diagrams (g, hz) in the presence of longitudinal field. From the top, $T = 0.1$, $h_x = 0.5$ [panel (a)], $T = 0.1$, $h_x = 1.5$ [panel (b)], $T = 0.8$, $h_x = 0.5$ [panel (c)], and $h_x = 1.5$ [panel (d)]. Nematic phase is present in the gray filled regions of the diagram. Nonconvergence occurs in the region filled with a square pattern.

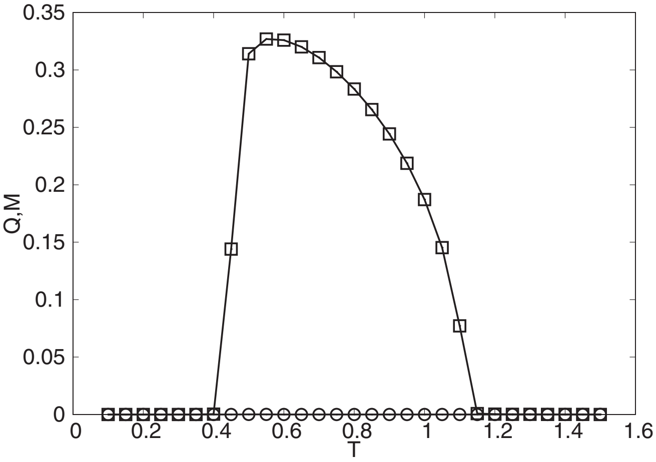

FIG. 17. Behavior of the orientational and translational order parameters for $h_x = 2.0$, $h_z = 0.1$, $J_2/J_1 = -1$. A range of temperatures where nematic order develops is observed. The latter certainly begins in a finite temperature ($T \approx 0.4$).

between the two orientations, positive and negative. Another remarkable feature is that the correlation between different stripes (dashed lines) are lower compared to that between elements of the same stripes (solid lines). As the transverse field increases, we approach the nematic phase, represented in Fig. 15(b). There we can observe a homogeneous magnetization, yet a clear remainder of the stripes is observed in the correlation structure. Even when both correlations are positive we can clearly see that the line joining sites of the same column are represented with wider lines than those between different stripes. This nematic phase breaks the rotational symmetry of the system and, in the case shown, it is translationally uniform. That is not necessarily the case if a larger system were considered, as randomly oriented nematic domains might appear. This would be more in correspondence with the use of the term nematic in quantum magnetism, where it names a phase for which the SU(2) symmetry is broken with no local order whatsoever.

Lastly, in Fig. 15(c) we observed the paramagnetic phase corresponding to $h_z = 0.76$, slightly beyond the transition point. Clearly, this paramagnetic phase is "polarized"(i.e., no zero net magnetization) due to the external magnetic field.

The behavior of the order parameters can be condensed in the h_z-g phase diagrams presented in Fig. 16 for different values of h_x and T. At low temperatures, Figs. 16(a) and 16(b)], it can be observed that the longitudinal field (h_x) changes the character of the transition. For example, in Fig. 16(a), corresponding to a low longitudinal field, we have a line of continuous and discontinuous transitions, with a critical point separating the two behaviors while in panel (b) (larger longitudinal field), all the transition line is discontinuous. So, we are tempted to associate the application of a larger longitudinal field with an increase in the discontinuous character of the phase transition. On the other hand, at higher temperatures, $T = 0.8$ [Figs. 16(c) and 16(d)], a nematic phase shows up penetrating the phase of stripes. As can be easily observed, this region broadens as we increase the value of the longitudinal field. On the other hand, we can check that as frustration increases ($|J_2/J_1|$), the longitudinal field required for the occurrence of the nematic phase is larger. Notice also that in panel (d), we have a nonconvergence region due to numerical

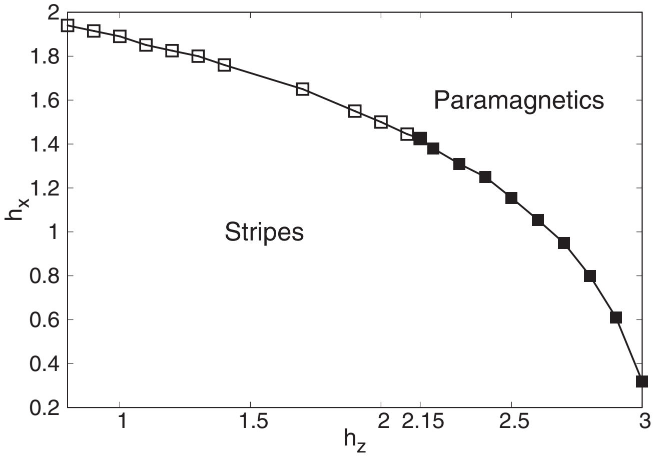

FIG. 18. h_z vs h_x phase diagram at low temperature ($T = 0.1$), and $J_2/J_1 = -1$. No nematic phase is present in this scenario. A critical point located around $h_z = 2.15$, $h_x = 1.425$ separates the transition line into two parts with respect to the order of the phase transition (first and second).

issues in the implementation, which is quite demanding in this region of the phase diagram.

These results suggest that the nematic phase does not appear in a low temperature scenario in agreement with results previously observed [40] in the classical model for $J_2/J_1 = -1$. To further support this, in Fig. 17, we show the behavior of the order parameters for $h_x = 2.0$. There we can clearly check that the nematic phase arises only after a certain threshold in T.

Another feature of these phase diagrams that is worth mentioning is the effect of h_x in the continuity of the phase transitions. The region in which first-order transitions occurs widens as h_x increases. This effect goes in the opposite direction to the one we observe under the application of a transverse field. In Fig. 18, we show the h_z vs h_x phase diagram for $T = 0.1$, $J_2/J_1 = -1$. The transition line is first order at low values of the transverse field, and large longitudinal one. In the other extreme case, a continuous transition occurs. The critical point is located around $h_z = 2.15$, $h_x = 1.425$.

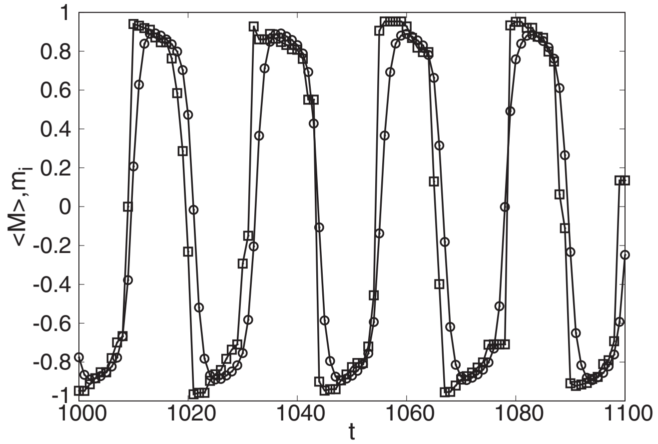

FIG. 19. Oscillatory behavior of the local magnetization of a single site (open squares), along with the global magnetization (open circles), in a lattice of 32 × 32 sites. The plot corresponds to the parameters $h_z = 0.8$, $T = 1.0$, $J_2/J_1 = -0.34$, deep inside a nonconvergence region.

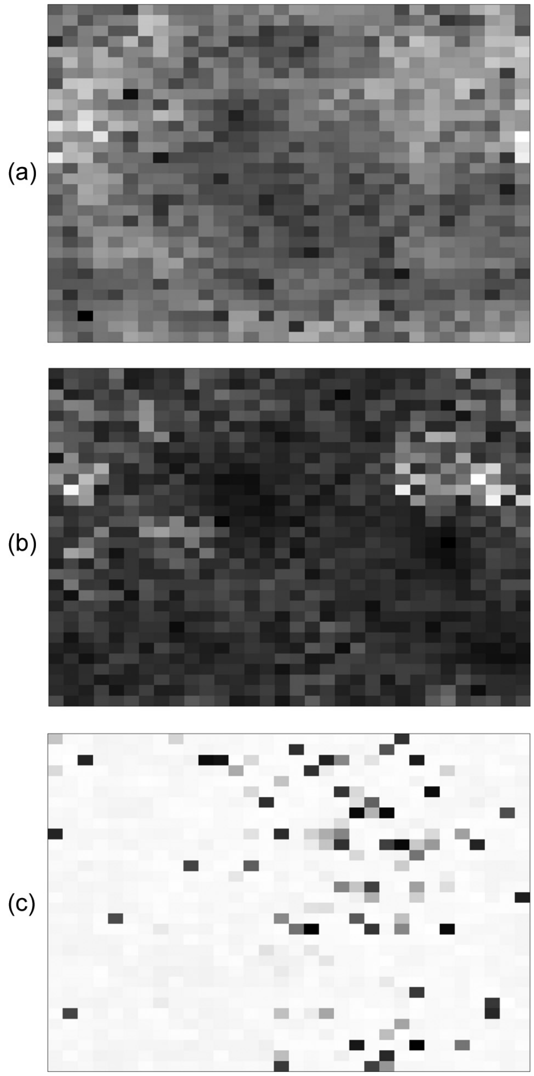

FIG. 20. Magnetization structure in a 32 × 32 lattice in a nonconvergence region for different time steps. The plot corresponds to the parameters $h_z = 0.8$, $T = 1.0$, $J_2/J_1 = -0.34$, deep inside a nonconvergence region. In all the time steps a general arrangement of the system favoring the mutual alignment of the spins is observed. In panel (c), the latter is particularly clear, as most of the sites show large positive magnetization. As in Fig. 15 we use a gray scale where positive magnetization appears as white.

V. CONCLUSIONS

In this work we studied the quantum J_1-J_2 model with nearest-neighbor ferromagnetic interactions ($J_1 \geqslant 0$) and next-nearest-neighbor antiferromagnetic interactions ($J_2 \leqslant 0$) in the presence of a transverse field using the quantum cluster variational method. We analyzed the model in an extensive lattice without particular assumptions about the symmetry of the problem. Our results show that quantum fluctuations

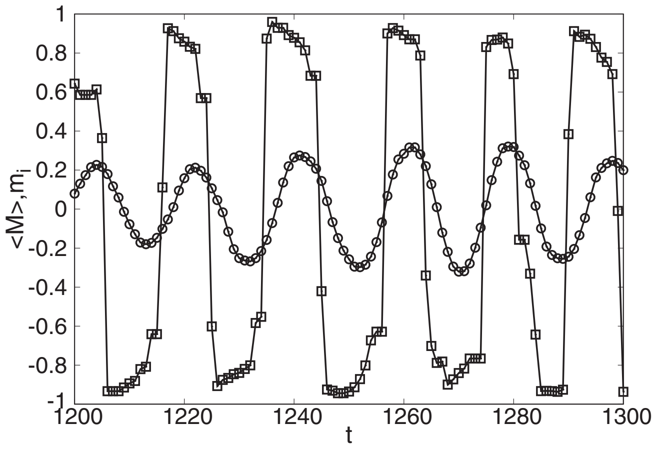

FIG. 21. Oscillatory behavior of the local magnetization of a single site (open squares), along with the global magnetization (open circles). The plot corresponds to the parameters $h_z = 0.8$, $T = 1.0$, $J_2/J_1 = -0.34$, deep inside a nonconvergence region in a lattice of 64×64 sites.

change the order of the transition; the larger the quantum effects the wider is the range of parameters for which the transition is continuous. Moreover, quantum fluctuations may induce a gap between the ferromagnetic phase and the phase of stripes and, in the presence of longitudinal fields, also a pronounced nematic phase that penetrates the phase of stripes. This nematic phase is characterized by the presence of orientational order and the lack of translational order. The phase diagrams presented in this paper in Secs. IV A and IV B are in qualitative agreement with previous results presented in literature [5,43,45,63]. In particular, numerical predictions of critical lines are in better agreement with Monte Carlo simulations than previous results obtained in the context of CMF and EFT approaches [4,63,64,68]. However, we leave open the definition of the critical point in the transition line between stripes and paramagnetic phase, where the previously noticed pseudo-first-order behavior [5,45,69], hides the real physics of the problem. On the other hand, we want to remark that as far as we know these are the first reports in the literature of the effect of a longitudinal field in the quantum version of the J_1-J_2 model. A careful quantum Monte Carlo study of this model, following the methods in [70,72] would help to elucidate these issues. Furthermore, similar results to those shown in Figs. 11 and 12 have been obtained by QMC simulations for a model of bosons in a frustrated lattice, which can be mapped to a J_1-J_2 Ising Hamiltonian in some cases [73].

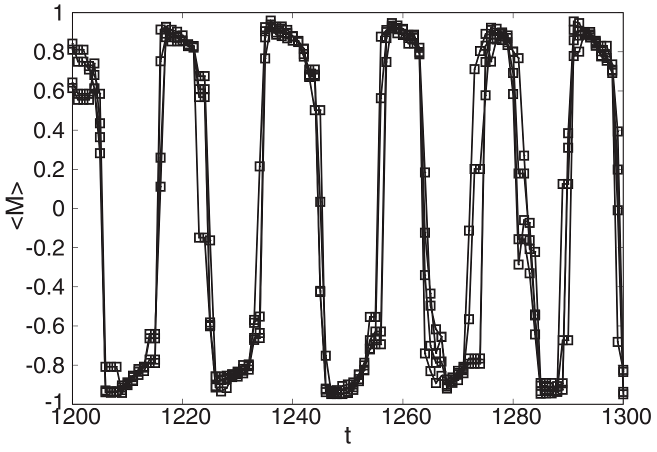

FIG. 22. Oscillatory behavior of the local magnetization of four sites close to one another, in a lattice of 64×64 sites. The plot corresponds to the parameters $h_z = 0.8$, $T = 1.0$, $J_2/J_1 = -0.34$, deep inside a nonconvergence region.

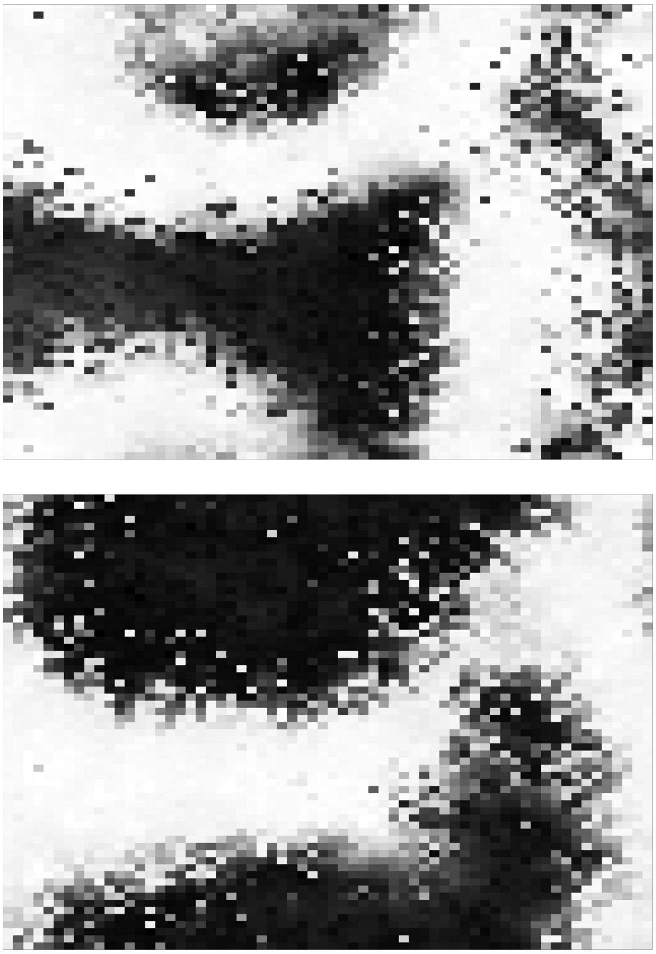

FIG. 23. Cluster formation in a 64×64 lattice in a nonconvergence region for two different time steps. The plot corresponds to the parameters $h_z = 0.8$, $T = 1.0$, $J_2/J_1 = -0.34$, $h_x = 0$ deep inside a nonconvergence region.

APPENDIX: ON THE CONVERGENCE OF QCVM NEAR THE CONTINUOUS-DISCONTINUOUS TRANSITION

Wide nonconvergence regions are observed in some of the T-$|J_2|/J_1$ phase diagrams in Fig. 12, as well as in the h_z-$|J_2|/J_1$ in Fig. 11. These nonconvergence regions are characterized by an oscillatory behavior of the system, which can be observed in Fig. 19. In this figure we show both the behavior of a single site magnetization as well as the global magnetization in a 32×32 lattice. Both values oscillate coherently, which is the signature of a global coordination rather than the result of single site isolated variations. An important thing to notice is that there is a decrease in the amplitude of the oscillations as we move from the ferromagnetic region to the paramagnetic one.

Oscillations in these zones are observed irrespective of the way in which we fill the initial conditions. Calculations were done in different ways in order to test this. On one hand, we perform the search for the equilibrium going from a convergence zone by using as initial condition always the previous equilibrium distributions of the effective fields. In this way, oscillations do appear with increasing amplitude as we move into the nonconvergence region until we approach the ferromagnetic region. Other calculations involve, for example, an initial breaking of the symmetry by applying an initial stronger field in some direction, and then turning it off after some iterations. In this way, a similar result is observed. By varying the damping of the algorithm in a range of reasonable values, only a change in the "period of oscillations" is observed, as would clearly be expected.

Figure 20 displays the magnetization structure of a 32 × 32 lattice inside the nonconvergence region. According to what was previously shown in Fig. 19, there is a large coordination between most of the sites of the lattice.

For much larger regions, say $L = 64$, both the global and local magnetization keep oscillating coherently, yet the global magnetization does it with a smaller amplitude (Fig. 21). This effect can be linked to the formation of clusters. In order to further motivate this statement we first show in Fig. 22 the oscillations of the magnetization of a site chosen randomly and some of its neighbors. We can observe what can be described as a local coordination. Finally, in Fig. 23, we show the 64 × 64 lattice structure for two different time steps. It can be directly observed in the two cases, the formation of clusters of sites pointing in the same direction, which visually shows what we supposed was the reason for the apparent contradiction in the oscillation of the local and global magnetization.

---

[1] S. Sachdev, *Quantum Phase Transitions* (Cambridge University Press, Cambridge, UK, 1999).

[2] E. Fradkin, *Field Theories of Condensed Matter Physics* (Cambridge University Press, Cambridge, UK, 2013).

[3] R. Shankar, *Quantum Field Theory and Condensed Matter Physics* (Cambridge University Press, Cambridge, UK, 2017).

[4] A. Bobák, E. Jurcisinová, M. Jurcisin, and M. Zukovic, Phys. Rev. E **97**, 022124 (2018).

[5] S. Jin, A. Sen, W. Guo, and A. W. Sandvik, Phys. Rev. B **87**, 144406 (2013).

[6] Y.-Z. Ren, N.-H. Tong, and X.-C. Xie, J. Phys.: Condens. Matter **26**, 115601 (2014).

[7] D. Yamamoto, Phys. Rev. B **79**, 144427 (2009).

[8] F. M. Zimmer, M. Schmidt, and J. Maziero, Phys. Rev. E **93**, 062116 (2016).

[9] A. Singhania and S. Kumar, Phys. Rev. B **98**, 104429 (2018).

[10] E. Domínguez and R. Mulet, Phys. Rev. B **97**, 064202 (2018).

[11] M. Mézard and A. Montanari, *Information, Physics and Computation* (Oxford University Press, Cambridge, 2009).

[12] T. Morita, Prog. Theor. Phys. **92**, 1081 (1994).

[13] T. Tanaka, K. Hirose, and K. Kurati, Prog. Theor. Phys. Suppl. **115**, 41 (1994).

[14] T. Rizzo, A. Lage-Castellanos, R. Mulet, and F. Ricci-Tersenghi, J. Stat. Phys. **139**, 375 (2010).

[15] E. Domínguez, A. Lage, R. Mulet, F. Ricci-Tersenghi, and T. Rizzo, J. Stat. Mech. (2011) P12007.

[16] A. Lage-Castellanos, R. Mulet, F. Ricci-Tersenghi, and T. Rizzo, J. Phys. A: Math. Theor. **46**, 135001 (2013).

[17] Z. W. E. Evans and A. M. Stephens, Phys. Rev. A **78**, 062317 (2008).

[18] M. Leifer and D. Poulin, Ann. Phys. **323**, 1899 (2008).

[19] D. Poulin and E. Bilgin, Phys. Rev. A **77**, 052318 (2008).

[20] E. Bilgin and D. Poulin, Phys. Rev. B **81**, 054106 (2010).

[21] D. Poulin and M. B. Hastings, Phys. Rev. Lett. **106**, 080403 (2011).

[22] F. G. Jouneghani, M. Babazadeh, D. Salami, and H. Movla, arXiv:1409.2048.

[23] I. Biazzo and A. Ramezanpour, J. Stat. Mech.: Theory Exp. (2013) P04011.

[24] I. Biazzo and A. Ramezanpour, Phys. Rev. E **89**, 062137 (2014).

[25] K. De' Bell, A. B. MacIsaac, and J. P. Whitehead, Rev. Mod. Phys. **72**, 225 (2000).

[26] R. Díaz-Méndez and R. Mulet, Phys. Rev. B **81**, 184420 (2010).

[27] S. Fey and K. P. Schmidt, Phys. Rev. B **94**, 075156 (2016).

[28] S. Fey, S. C. Kapfer, and K. P. Schmidt, Phys. Rev. Lett. **122**, 017203 (2019).

[29] A. Mendoza-Coto, D. A. Stariolo, and L. Nicolao, Phys. Rev. Lett. **114**, 116101 (2015).

[30] A. Mendoza-Coto, D. G. Barci, and D. A. Stariolo, Phys. Rev. B **95**, 144209 (2017).

[31] A. Mendoza-Coto, Danilo Emanuel Barreto de Oliveira, L. Nicolao, and R. Díaz-Méndez, Phys. Rev. B **101**, 174438 (2020).

[32] S. A. Cannas, M. F. Michelon, D. A. Stariolo, and F. A. Tamarit, Phys. Rev. B **73**, 184425 (2006).

[33] R. M. Nandkishore and S. L. Sondhi, Phys. Rev. X **7**, 041021 (2017).

[34] V. Oganesyan and D. A. Huse, Phys. Rev. B **75**, 155111 (2007).

[35] G. M. Bruun and E. Taylor, Phys. Rev. Lett. **101**, 245301 (2008).

[36] M. M. Parish and F. M. Marchetti, Phys. Rev. Lett. **108**, 145304 (2012).

[37] J. L. Morán-López, F. Aguilera-Granja, and J. M. Sanchez, Phys. Rev. B **48**, 3519 (1993).

[38] J. L. Moran-Lopez, F. Aguilera-Granja, and J. M. Sanchez, J. Phys.: Condens. Matter **6**, 9759 (1994).

[39] A. I. Guerrero, D. A. Stariolo, and N. G. Almarza, Phys. Rev. E **91**, 052123 (2015).

[40] E. Domínguez, A. Lage-Castellanos, C. Lopetegui, and R. Mulet, Rev. Cubana Fís. **36**, 20 (2019).

[41] R. A. dos Anjos, J. R. Viana, and J. R. de Sousa, Phys. Lett. A **372**, 1180 (2008).

[42] A. Kalz, A. Honecker, S. Fuchs, and T. Pruschke, Eur. J. Phys. B **65**, 533 (2008).

[43] A. Kalz, A. Honecker, S. Fuchs, and T. Pruschke, J. Phys.: Conf. Ser. **145**, 012051 (2009).

[44] A. Kalz, A. Honecker, and M. Moliner, Phys. Rev. B **84**, 174407 (2011).

[45] S. Jin, A. Sen, and A. W. Sandvik, Phys. Rev. Lett. **108**, 045702 (2012).

[46] Y. Kohama, H. Ishikawa, A. Matsuo, K. Kindo, N. Shannon, and Z. Hiroi, Proc. Natl. Acad. Sci. U.S.A. **116**, 10686 (2019).

[47] N. Shannon, B. Schmidt, K. Penc, and P. Thalmeier, Eur. Phys. J. B **38**, 599 (2004).

[48] F. Mezzacapo, Phys. Rev. B **86**, 045115 (2012).

[49] H.-C. Jiang, H. Yao, and L. Balents, Phys. Rev. B **86**, 024424 (2012).

[50] E. Dagotto and A. Moreo, Phys. Rev. Lett. **63**, 2148 (1989).

[51] R. Shindou, S. Yunoki, and T. Momoi, Phys. Rev. B **87**, 054429 (2013).

[52] T. P. Cysne and M. B. S. Neto, Europhys. Lett. **112**, 47002 (2015).

[53] P. Carretta, N. Papinutto, C. B. Azzoni, M. C. Mozzati, E. Pavarini, S. Gonthier, and P. Millet, Phys. Rev. B **66**, 094420 (2002).

[54] R. Melzi, S. Aldrovandi, F. Tedoldi, P. Carretta, P. Millet, and F. Mila, Phys. Rev. B **64**, 024409 (2001).

[55] R. Nath, A. A. Tsirlin, H. Rosner, and C. Geibel, Phys. Rev. B **78**, 064422 (2008).

[56] A. Orlova, E. L. Green, J. M. Law, D. I. Gorbunov, G. Chanda, S. Krämer, M. Horvatić, R. K. Kremer, J. Wosnitza, and G. L. J. A. Rikken, Phys. Rev. Lett. **118**, 247201 (2017).

[57] J. Yedidia, W. T. Freeman, and Y. Weiss, IEEE Trans. Inf. Theory **51**, 2282 (2005).

[58] R. Kikuchi, Phys. Rev. **81**, 988 (1951).

[59] The diagonal interactions do not belong to any overlap region and therefore, according to the CVM, they do not appear explicitly as independent terms in the approximated free energy.

[60] Notice that λ and γ are actually operators on the Hilbert space of the pairs l and the single spins s, respectively.

[61] In certain cases the algorithm fails to converge. This will be discussed afterwards together with the numerical results.

[62] Actually, what is usually stored is a weighted sum of the new and the old values. This procedure introduces a kind of *damping* that might help convergence.

[63] N. Kellermann, M. Schmidt, and F. M. Zimmer, Phys. Rev. E **99**, 012134 (2019).

[64] T. Balcerzak, K. Szałowski, A. Bobák, and M. Žukovič, Phys. Rev. E **98**, 022123 (2018).

[65] L. Onsager, Phys. Rev. **65**, 117 (1944).

[66] H. A. Bethe, Proc. R. Soc. A **150**, 552 (1935).

[67] R. Peierls, Math. Proc. Cambridge Phil. Soc. **32**, 477 (1936).

[68] A. Bobák, T. Lučivjanský, M. Borovský, and M. Žukovič, Phys. Rev. E **91**, 032145 (2015).

[69] A. Kalz and A. Honecker, Phys. Rev. B **86**, 134410 (2012).

[70] B. K. Chakrabarti, A. Dutta, and P. Sen, *Quantum Ising Phases and Transitions in Transverse Ising Models*, Lecture Notes in Physics Monographs Vol. 41 (Springer-Verlag, Berlin, Heidelberg, 1996).

[71] P. Chandra, P. Coleman, M. A. Continentino, and G. G. Lonzarich, Phys. Rev. Research **2**, 043440 (2020).

[72] R. Moessner and S. L. Sondhi, Phys. Rev. B **63**, 224401 (2001).

[73] A. Kalz, A. Honecker, S. Fuchs, and T. Pruschke, Phys. Rev. B **83**, 174519 (2011).